Serb. Astron. J. (2026), OnLine-First
DOI: https://doi.org/10.2298/SAJ251106002M

UDC 524.74 : 519.876
Original scientific paper

POSSIBLE ORBITS OF A SATELLITE GALAXY FOR SHELL FORMATION IN GALAXY MERGER EVENTS

S. Milošević

University of Belgrade, Faculty of Mathematics, Department of Astronomy, Studentski trg 16, 11000 Belgrade, Serbia

E–mail: *stanislav.milosevic@matf.bg.ac.rs*

(Received: November 6, 2025; Accepted: February 25, 2026)

SUMMARY: We investigated formation of stellar shells in mergers between the host spiral galaxy and its satellite galaxy in different scenarios. Results of previous works showed that stellar shells are formed in very radial mergers. We run *N*-body simulations for 4 Gyrs, with an M31-like host galaxy and spherical satellite. The simulations start with zero radial velocity. We found that the initial tangential velocities of 50 km/s and higher, in these merger scenarios, define orbits where stellar shells are not prominent in comparison with almost radial mergers. With a deviation from a very radial orbit defined with zero initial velocity, it is possible to have stellar shells formed with initial velocity up to 50 km/s for initial distance of 150 kpc, then for distance of 200 kpc with velocity up to 25 km/s, and for 250 kpc initial distance, stellar shells are formed only in a radial merger, after 2.5 Gyrs from the beginning of the simulation. With initial velocities higher than 100 km/s, we do not have stellar shells formation in these scenarios.

Key words. Galaxies: interactions – Galaxies: kinematics and dynamics – Methods: numerical

1. INTRODUCTION

In the standard hierarchical picture of structure formation, large massive galaxies are formed in merger events of the smaller galaxies and their mass can grow by star formation and interstellar gas accretion (White and Rees 1978, White and Frenk 1991, Cole et al. 2000). These mergers are led by local overdensities and can produce galaxies with different morphologies, masses, metallicity distribution, gas content, and other properties. These morphological differences are noticed in many galaxy surveys (Dressler 1980, Tempel et al. 2011). The survived small-mass galaxies, in many cases became satellite galaxies of large, massive spiral and elliptical galaxies (Klypin et al. 1999, Moore et al. 1999). These galaxies can be accreted onto the large massive galaxy, their host. The results of these merger events can be structures formed in the halo of the host, in the case of smaller satellites, as well as the remnant of the satellite, which we can detect as a globular cluster or local stellar overdensity, if the core of the satellite survives that merger event (Bullock and Johnston 2005, Belokurov et al. 2006, Kruijssen et al. 2020). That can be possible due to specific circumstances of the merger and the timescale of the event. Sometimes, after several orbits, the satellite galaxy is completely disrupted (Ibata et al. 1994, Johnston et al. 1999).

On its orbit around the host, the satellite galaxy is losing its stellar and gas material due to tidal friction, and it forms tidal structures. These structures, such as stellar streams and shells, depend on properties of the satellite as well as merger timescale, and orbit properties (Johnston et al. 1996, Bullock and Johnston 2005, Cooper et al. 2010). In the other direction, these structures are smoking guns of galaxy interactions, and their properties are important to reproduce the merger history and properties of the progenitor, satellite galaxy.

In the last several decades, shells have been detected in galaxies of different morphological types (Arp 1966, Schweizer and Ford 1985). In many recent observational studies, shell galaxies are reported (e.g. Bílek et al. 2016). Stellar shells are low surface brightness tidal structures and are not easy to detect. Also, due to different merger scenarios, shells can have various morphological differences. Shells are mostly observed in elliptical galaxies (Atkinson et al. 2013), but there are also reported shells in halos of spiral galaxies (Martínez-Delgado et al. 2010, de Blok et al. 2014). Stellar streams and shells are observed in nearby galaxies and in the Milky Way (MW). The proximity of the M31 galaxy gives us an opportunity for high-precision observations of these faint structures. Shells in M31 are discovered by Ferguson et al. (2002). Metallicities of the North-east shell are given in Escala et al. (2021). Measured properties for the Western shell are given in Fardal et al. 2007, 2012.

Many theoretical works were done to explain formation of tidal structures in halos of large massive galaxies. In the work of Quinn (1984), it is shown that shells could be formed in a merger event of a massive host galaxy and a small satellite. Radial mergers as events leading to a shell formation were presented in Hernquist and Quinn 1988, 1987, 1989, Ebrová et al. 2012, Bílek et al. 2022, Valenzuela and Remus 2024. Properties of the shells and their possible origins are reviewed in Ebrova (2013). A major merger scenario was also investigated, e.g., N-body and hydrodynamic simulations were done in the work of Petersson et al. (2023). The analyses of cosmological simulation (Pop et al. 2018) suggest that a radial merger is necessary for shell formation in merger scenarios with small satellite galaxies. A radial merger will form stellar shells, while non-radial will form stellar streams (Amorisco 2015). The properties of shells could give us constraints on merger properties (Ebrová et al. 2020). The dependence of formed structures on properties of satellites was presented in Karademir et al. (2019) and Milošević (2022), refered to as Paper I. In this paper, we investigated the influence of morphology and orbital inclination, and the direction of rotation of the host disk, on formation of tidal structures in the halo of an M31-type spiral galaxy. We used N-body simulations to analyze merger events, where we had two models of satellite galaxies: a spiral and spherical satellite at the same initial distance from the center of the host. In both cases of merger models, the initial velocity of the satellite was zero, which led to highly radial mergers. We vary the morphology and orbit inclination for the same mass of the satellite.

In this paper, we investigate the orbits of the satellite that can produce shell structures in the halo of the host. We employed the N-body models for both the host and satellite galaxies and investigated various merger scenarios for the first 4 Gyrs after the beginning of simulation. This time interval is motivated by the estimate of the time interval for forming tidal structures in M31 halo, which is between 2 and 3 Gyrs (Hammer et al. 2018, Milošević et al. 2022). For the same models given in Paper I, a satellite with the same mass, we vary the initial distances and initial tangential velocities of the satellites. Different velocities will produce different orbits. With a larger velocity, the merger will be less radial, and we can then find the range of velocities for which shell formation occurs in the halo of the host. We investigated how different initial velocities affect the morphology of shells and streams that are formed by tidal disruption of the satellite galaxy. Given observations of stellar shells – whether faint or prominent, at different radii, and occurring as single or multiple structures – we can constrain the initial position and the range of initial velocities of the satellite galaxy that can lead to the formation of the observed shells in merger events. In other words, we can find non-radial merger scenarios in which prominent or faint stellar shells can be formed, and give the possible parameters for initial conditions of merger events.

This paper is organized as follows: in Section 2, we present N-body models for the host galaxy and satellite, as well as the initial properties of satellite orbits in merger events. In Section 3, we present the main results of merger events, formed structures in different merger scenarios, while the discussion and conclusion are given in Section 4.

2. METHODS

For the host galaxy, we used an M31-like galaxy with three main components: the bulge, disk, and dark matter halo. This model is the same one we used in Paper I. For the satellite galaxy, we also used the model described in Paper I. We took a spherical satellite that consists of a spherical bulge and a dark matter halo. The N-body models of galaxies are generated with the GalactICs package (Widrow et al. 2008). We used the same density profiles for the disk, bulge, and halo, as in previous works (Geehan et al. 2006, Sadoun et al. 2014, Milošević et al. 2022, Milošević 2022). The parameters for the density profiles of the host components correspond to the M31 galaxy model used in Milošević et al. (2022) and Paper I, while the parameters for the satellite galaxy are the same as in Paper I.

The bulge is represented with the Prugniel-Simien profile (Widrow et al. 2008):

$$\rho_{\rm b} = \rho_{\rm b0} \left(\frac{r}{r_{\rm b}}\right) \exp\left(r/r_{\rm b}\right)^{-1/n} . \qquad (1)$$

Here, $\rho_{\rm b0}$ is the density at $r = r_{\rm b}$, and $r_{\rm b}$ is the scale radius for the bulge.

The disk is represented by a combination of two profiles: an exponential profile of surface density in the x-y plane, and a sech^2 law in the vertical z-direction, where the x-y plane is the plane of the host galaxy disk. The exponential profile is given with (Geehan et al. 2006, Sadoun et al. 2014):

$$\Sigma(R) = \frac{M_{\rm d}}{2\pi R_{\rm d}^2} e^{-\frac{R}{R_{\rm d}}}. \quad (2)$$

Here, $M_{\rm d}$ is the total mass of the disk, Σ is the surface density, and $R_{\rm d}$ is the disk scale radius. In the last two equations, r is the spherical radius, and R is the cylindrical radius.

The sech^2 profile is used in the vertical z-direction (Sadoun et al. 2014), and the combined profile is given by:

$$\rho(R,z) = \frac{\Sigma(R)}{2z_0} {\rm sech}^2\left(\frac{z}{z_0}\right). \quad (3)$$

Here, z_0 is the scale height of the disk.

A spherical dark matter halo is represented in the form of the Navarro-Frenk-White profile (Navarro et al. 1996) given in GalactICs (Widrow et al. 2008):

$$\rho(r) = \frac{2^{2-\alpha}\sigma_{\rm h}^2}{4\pi r_{\rm s}^2} \frac{1}{(r/r_{\rm s})^{\alpha}(1+r/r_{\rm s})^{3-\alpha}} \frac{1}{2} {\rm erfc}\left(\frac{r-r_{\rm h}}{\sqrt{2}\delta_{r_{\rm h}}}\right). \quad (4)$$

Here, all parameters are the same as in Milošević et al. (2022) and Paper I: $r_{\rm h}$ is the radius of halo where the density starts to decrease, $\sigma_{\rm h}$ is a typical velocity, $\delta_{r_{\rm h}}$ is the distance at which the density falls to zero, $r_{\rm s}$ is the scale radius for halo, and α is an exponent in the NFW profile and we took $\alpha = 1$.

For the satellite galaxy, we used the spherical model. This model has profiles for the bulge and dark matter, also represented with Eqs. (1) and (4). Parameters used for generating models of galaxies are given in Table 1.

We simulated different orbits of the satellite galaxy in merger events. We set up three initial positions for the satellite galaxy in the plane of the disk, with initial distances of 150, 200, and 250 kpc. For each initial position, we attached tangential velocities of 0, 25, 50, 75, 100, and 150 km/s, where the velocity vector is normal to the radial distance from the host. The initial positions are settled along the x-axis, and the velocity vector is in the plane of the host disk, oriented along the positive direction of the y-axis, while the disk rotates counterclockwise (from the x-axis towards the y-axis). Since we concluded in Paper I that streams and shells could be formed with different morphologies of the satellite, given zero initial velocity, we adopted only the spherical model in this paper and investigated different initial velocities. To run simulations, we used the cosmological simulation code Gadget2 (Springel 2005). We took pure N-body models with particle mass resolution of $10^5 M_\odot$ and $10^6 M_\odot$ for baryonic and dark matter for the host, and $10^4 M_\odot$ for the satellite. The stellar to halo mass ratio is consistent with the stellar to halo mass relation given in Behroozi et al. (2013). The concentration parameter c for the host and satellite is given in Table 1. Masses of particles and numbers of particles for each component are also given in Table 1. For simulations, we used a softening length of 0.1 kpc, and we ran simulations for 4 Gyrs.

3. RESULTS

In merger events, we follow the disruption of the satellite galaxy in the gravitational potential of the host. For each initial position, we defined initial velocity and investigated the formation of the stellar structures in the halo of the host. We investigated the formation of these structures in simulations that last for 4 Gyrs. In previous works, we showed that for a similar merger setup, the structures are formed in the first 3 Gyrs after the beginning of simulation.

In Fig. 1, we presented the merger event for the S3-150-0 model. The name S3-150-0 means that we use a spherical satellite, in the x-y plane, that is, in the plane of the disk of the host, at initial distance of 150 kpc, along the x-axis, with zero initial velocity (the second number). This model is consistent with previous works. A spherical satellite on radial orbit with zero initial velocity is disrupted by the tidal force. As this is a radial merger, we have formed stellar shells, and a significant part of the mass consists of the shells. After each pericentric passage, we have several shells formed. In Fig. 2, the same merger is presented only in the x-y plane, unlike Fig. 1, where this merger is presented in the x-z plane. The bottom row in these two figures has a smaller scale for better representation of the central region.

This model is used to compare shell forming in the merger events with non-zero initial velocities. The results of the merger event for the S3-150-50 scenario are presented in Fig. 3 and Fig. 4. In this model, we have the initial velocity of 50 km/s, and we can see formed streams in the x-z plane in Fig. 4 and faint shells in Fig. 3. We can see the differences, for example, after 2 Gyrs from the beginning of the simulation in Fig. 1 and Fig. 3, or Fig. 2 and Fig. 4, where in the case of the radial merger, the tidal structures are already formed, while in the case of non-zero initial velocity, these structures are not yet formed. This is the reason to investigate several different initial velocities for the same distance in order to find the value above which are not formed shells, in other words, to find a possible deviation from the radial orbit where we still have shells after a reasonable time from the beginning of the simulation.

We compare all the merger scenarios after 2.5 Gyrs from the beginning of the simulation in Fig. 5 and Fig. 6. In both figures, the first row corresponds to the initial distance of 150 kpc, the middle to 200 kpc, and the bottom to 250 kpc. Each panel from left to right represents a merger event with initial velocity from 0 to 100 km/s. We presented only the baryonic matter in the x-z plane in Fig. 5, and in the x-y plane in Fig. 6. The host particles are presented in yellow color, and satellite particles in blue. From these two figures at the moment of 2.5 Gyrs from the begin-

Table 1: The values of the parameters for the N-body models of the progenitor, satellite galaxy, and host M31-like galaxy.

Satellite galaxy component	$m_{particle}$ $[M_\odot]$	N			
Baryonic matter	1.68×10^4	131072	$r_{\rm b} = 1.03$ kpc	$\sigma_{\rm b} = 93$ km/s	$M_{\rm s} = 2.2 \times 10^9 M_\odot$
Dark matter halo	9.86×10^4	248809	$r_{\rm h} = 45$ kpc	$\sigma_{\rm h} = 185$ km/s	$M_{\rm h} = 2.45 \times 10^{10} M_\odot$
			$r_{\rm s} = 5$ kpc	$\delta_{r_{\rm h}} = 6$ kpc	c = 10.2
Host galaxy component	$m_{particle}$ $[M_\odot]$	N			
Bulge	3.36×10^5	96247	$r_{\rm b} = 1{,}23$ kpc	$\sigma_{\rm b} = 393$ km/s	$M_{\rm b} = 3.2 \times 10^{10} M_\odot$
Disk	3.36×10^5	108929	$R_{\rm d} = 6.82$	$z_0 = 0.57$	$M_{\rm d} = 3.66 \times 10^{10} M_\odot$
Halo	3.36×10^6	261905	$r_{\rm h} = 122.5$ kpc	$r_{\rm s} = 8$ kpc	$M_{\rm h} = 8.8 \times 10^{11} M_\odot$
			$\delta_{r_{\rm h}} = 12$ kpc	$\sigma_{\rm h} = 525$ km/s	c = 16.8

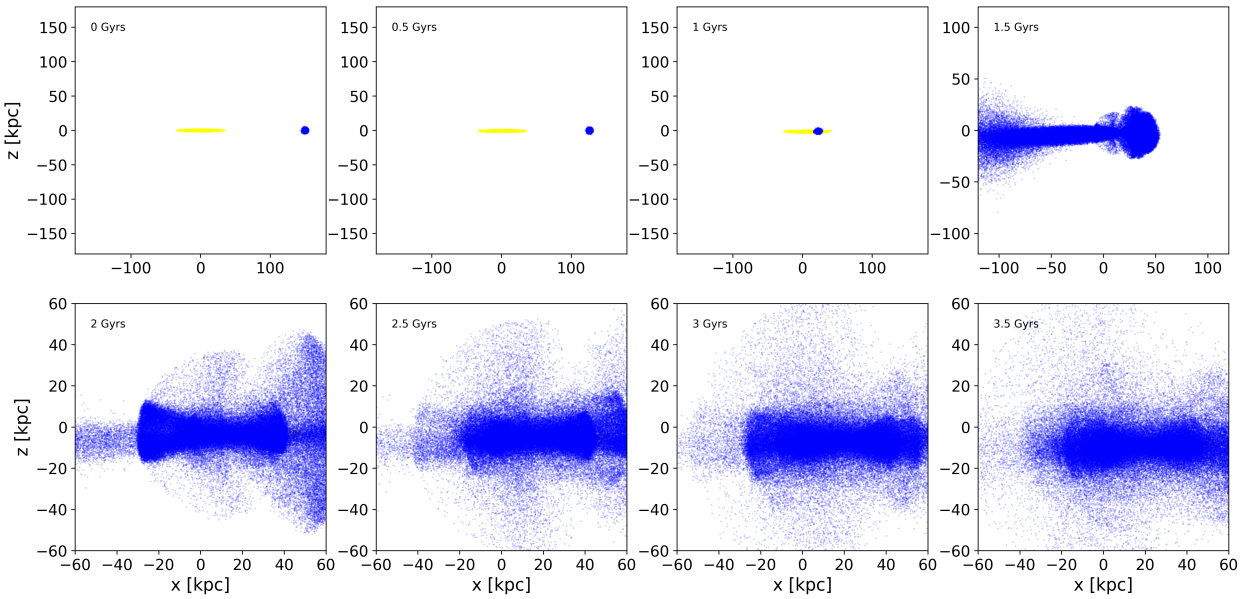

Fig. 1: The merger in the S3-150-0 scenario in the x-z plane from 0 to 3.5 Gyrs due to the suggestion from previous works (Sadoun et al. 2014, Milošević 2022). The disk of the host is represented in yellow, and the baryonic matter of the satellite in blue. We can see the formed streams and stellar shells after several pericentric passages.

ning of the simulation, it is clear that multiple shells and streams are formed in the radial scenario where the initial velocity of the satellite galaxy is zero. For the initial distance of 150 kpc, these tidal structures are more prominent since the satellite galaxy, and later remnant of the satellite, passes several times near the central region of the host so that more mass is stripped off and deposited in the tidal structures. In the merger events, where the orbit deviates from the radial, with initial velocities of 25 and 50 km/s, stellar shells fare formed for the initial distance of 150 kpc. For the same distance and velocities of 75 and 100 km/s, the satellite galaxy will make several orbits and will be tidally deformed, but without disruption that will lead to stellar shells formation in the first 2.5 Gyrs of interaction with the host. For an initial distance of 200 kpc, tidal structures formed for initial velocities of 0 and 25 km/s. In Fig. 6, we can see formed shells for 25 km/s initial velocity (the middle row, second panel), and with initial velocity, from 50 km/s and larger, there is a lack of tidal structures. A satellite galaxy will make an orbit around the host, and some tidal tails can be made from the stellar material of the host, as is presented in Fig. 6 for the initial distance of 200 kpc, and initial velocity 75 km/s. In this situation, the satellite will pull the material from outer part of the host galaxy. With increasing the initial distance to 250 kpc, we can conclude that shells are formed only for zero initial velocity. The differences between models are influenced by different impact times, which is a result of different initial positions and velocities.

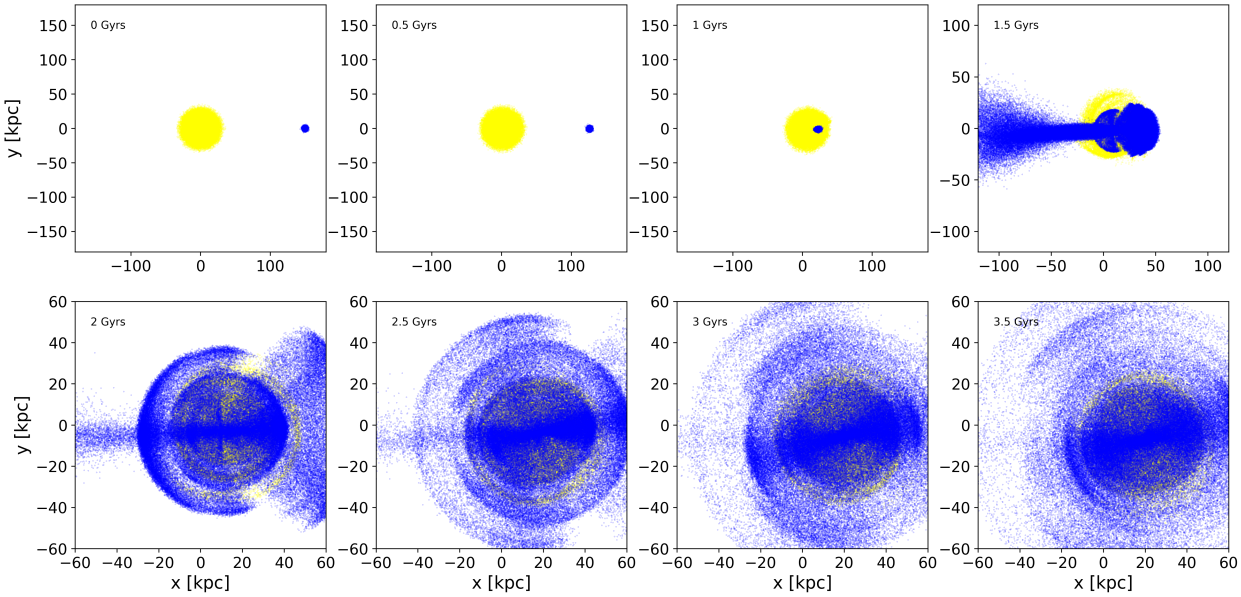

Fig. 2: The merger in the S3-150-0 scenario in the x-y plane from 0 to 3.5 Gyrs. Colors and symbols are the same as in Fig. 1.

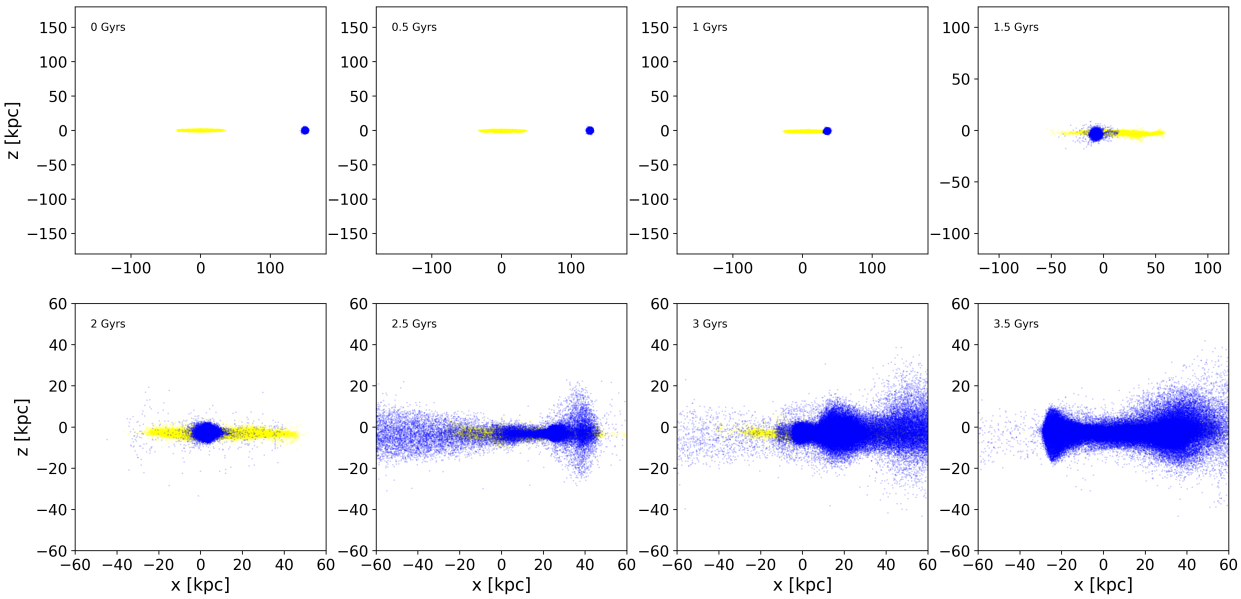

Fig. 3: The merger event for the scenario S3-150-50. In this scenario, the initial velocity is 50 km/s normal to the direction of the host-satellite, oriented in the y-direction. We can see that stellar shells and streams are not yet formed after 2 Gyrs.

In Fig. 7 and Fig. 8, we presented the evolution of tidal structures in merger events after 1 Gyr after the first pericentric passage. Fig. 7 and Fig. 8 show mergers in the x-z and x-y plane, respectively. For the S3-150 models, we have formed structures up to 75 km/s of initial tangential velocity. For the S3-200 models, structures are formed up to 50 km/s, and for the S3-250 models, only in the radial merger. Since we compare moments after a fixed time from the first passage near the pericenter, we will have a more promeninent shell in the case of radial mergers for all three different distances since, in this situation, we excluded the influence of the initial distance. We can see a clear difference between the first panel in the bottom row in Fig. 6 and corresponding panel in Fig. 8.

The formed shells and streams can better be seen in the v-d phase plots, where v is the radial velocity, and d is radial distance from the center of the host. Fig. 9 and Fig. 10 present the v-d plots for models

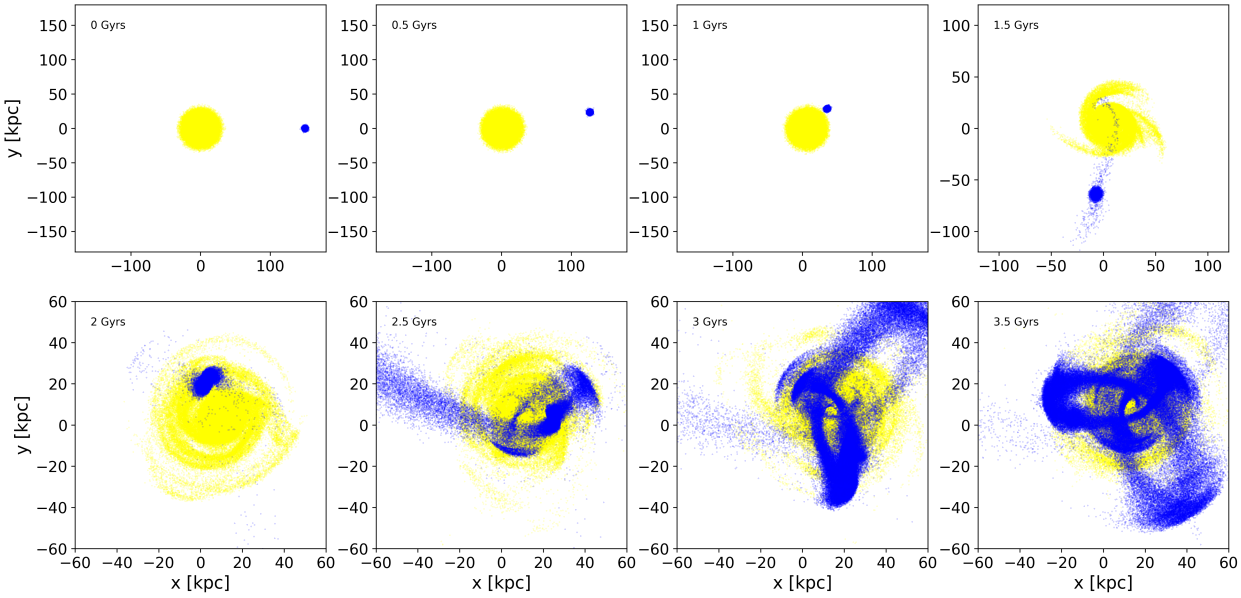

Fig. 4: The merger history for the S3-150-50 model in the x-y plane. We can see the formed stellar streams, but no prominent shells.

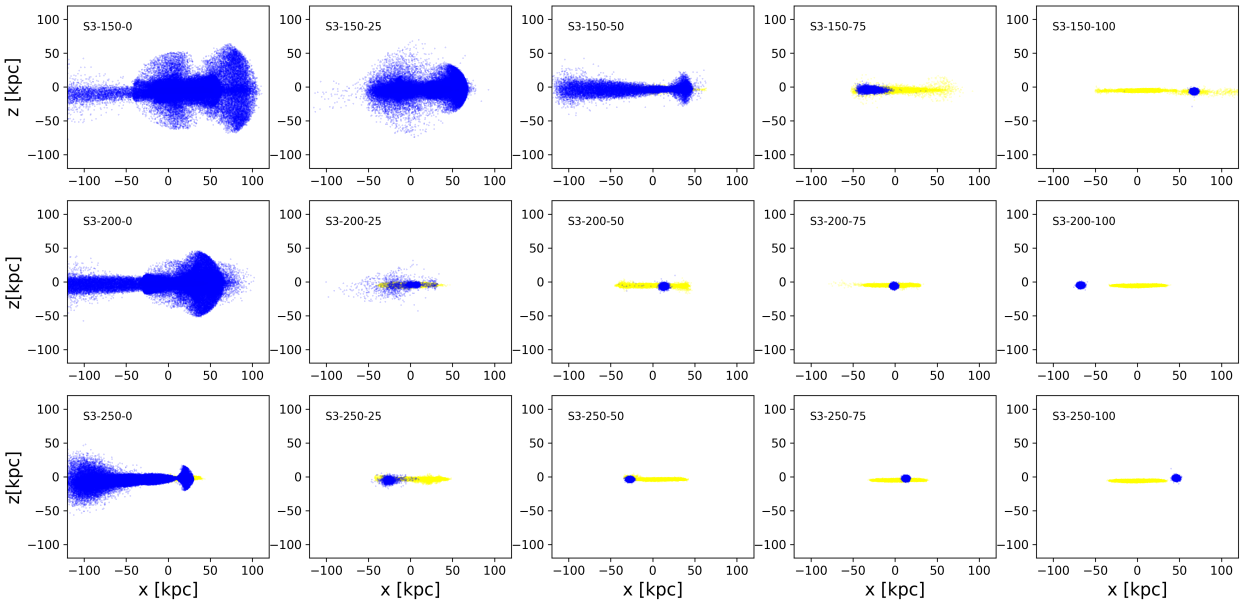

Fig. 5: Different merger scenarios at 2.5 Gyrs from the beginning of the simulation. The upper row represents models with initial distance of 150 kpc for initial velocities from 0 to 100 km/s with a step of 25 km/s. The middle row is for models with initial distance of 200 kpc, and the bottom row is for initial distance of 250 kpc. The merger events are represented in the x-z plane, and only the baryonic matter is presented. The disk of the host is represented in yellow, and the baryonic matter of the satellite in blue.

S3-150-0 and S3-150-50 for the time interval from 0 to 3 Gyrs. In the first case, we can see formed shells and a stellar stream as well. In Fig. 10, we can see a very faint structure of one shell, unlike multiple shells in Fig. 9. In this merger event, the remnant of the galaxy due to the non-radial orbit, survives after 3 Gyrs, and less material is left for the shells. Prominent shells exist after 2.5 Gyrs, which can be seen in Fig. 9 in the middle panel in the bottom row, and the faint shells in the corresponding panel in Fig. 10. The same comparison can be seen in Fig. 1 and Fig. 2 for the S3-150-0 model, and in Fig. 3 and Fig. 4 for the S3-150-50 model, which corresponds to Fig. 10 in the phase space. In Fig. 11, a v-d plot is presented

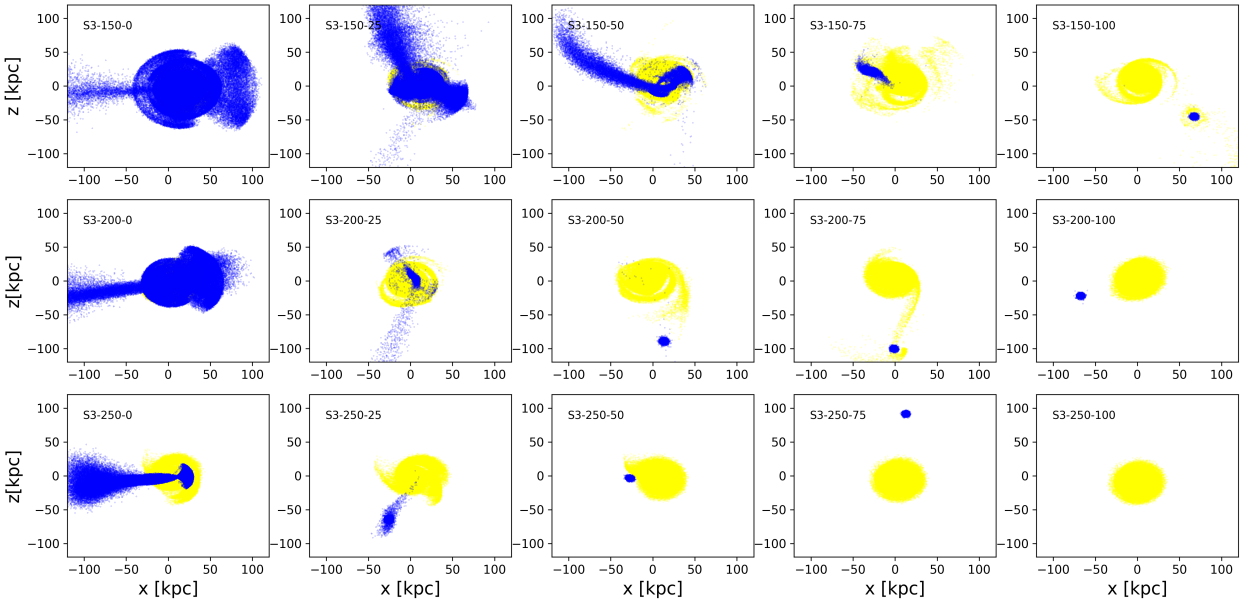

Fig. 6: Different merger scenarios at 2.5 Gyrs from the beginning of the simulation. Panels represent the same models as given in Fig. 5, but in the x-y plane. Symbols are the same as in Fig. 5.

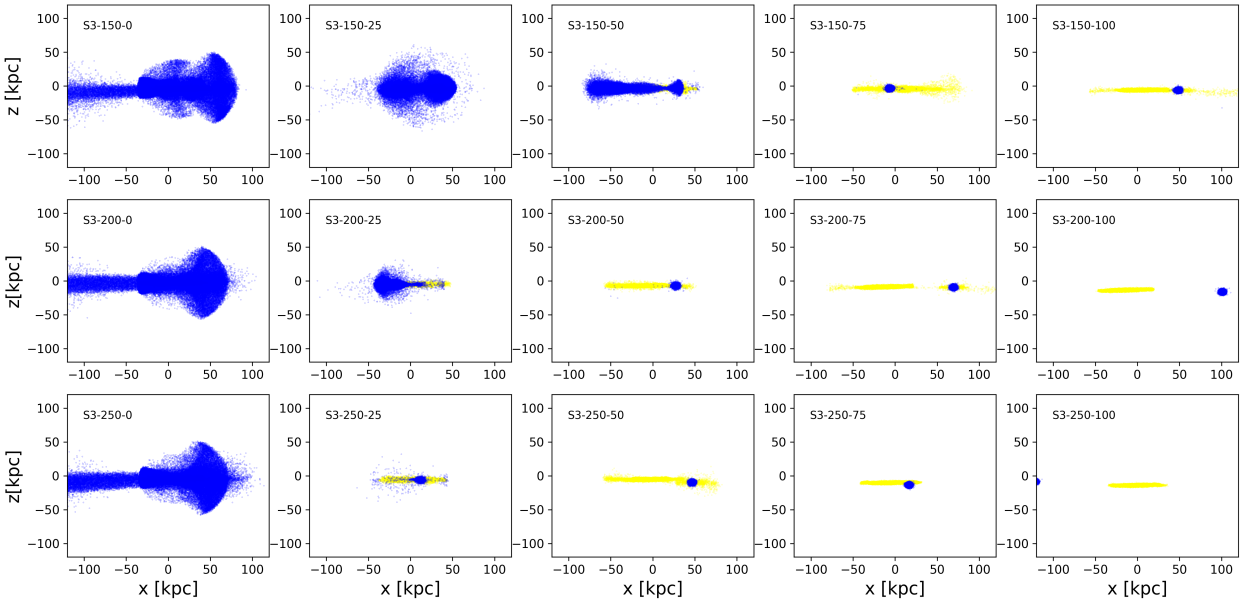

Fig. 7: Different merger scenarios at at 1 Gyr after the first pericentric passage. Panels represent the same models as given in Fig. 5, in the x-z plane. Symbols are the same as in Fig. 5.

for the same time interval for the S3-150-100 model. In this case, for the 100 km/s of initial velocity, the satellite galaxy is orbiting around the host, without a merger for the first 3 Gyrs.

The v-d plots for all models after 2.5 Gyrs are given in Fig. 12. Panels in the figure correspond to the panels in Fig. 5 and Fig. 6. In Fig.12, we have confirmation of what was previously stated: shells are formed in radial merger events for all models, and we also have formed shells exist for models S3-150 for initial velocities up to 50 km/s; for the model S3-200 up to 25km/s, and for S3-250 only in the radial merger with zero velocity. These shells are different in their radii and intensity. With the increase of initial velocity, the number of shells and their radii decreases. Shells are becoming less prominent due to a smaller number of particles forming shells. For the S3-150 model, the radial merger produces several very

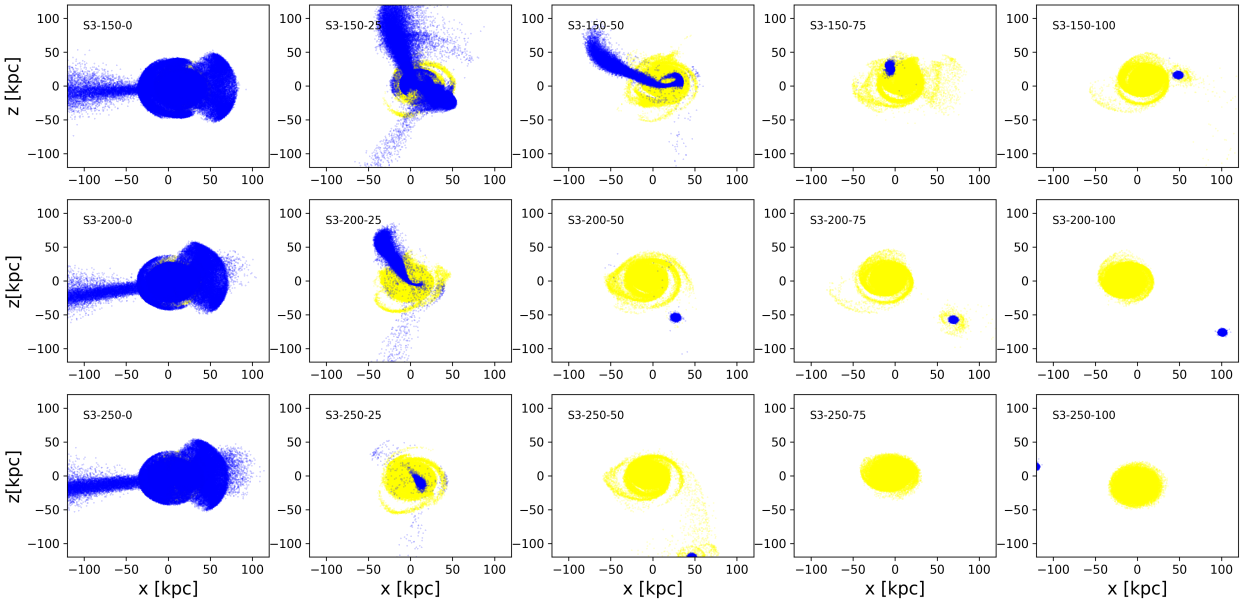

Fig. 8: Different merger scenarios at 1 Gyr after the first pericentric passage. Panels represent models as given in Fig. 5, in the x-y plane. Symbols are the same as in Fig. 5.

prominent shells with radii of up to 100 kpc, while in the S3-150-50 model the number of shells, as well as their intensity and radii, are smaller. Similarly, if we compare S3-200-0, S3-200-25, and S3-200-50, we can see very faint shells for S3-200-25, and no formed shell for the S3-200-50 model. In Fig. 13, we presented the v-d plots at 1 Gyr after the first pericentric passage in each simualation. Panels correspod to panels in Fig. 7 and Fig. 8. We can confirm the formation of the previous results presented in Fig. 12, and formation of prominent shells in radial mergers for different initial distances. For a fixed distance, the shell will be less prominent and will not form for initial velocities larger than 50 km/s for S3-150 models, 25 km/s for S3-200 models, and 0 km/s for S3-250 models.

4. DISCUSSION AND CONCLUSIONS

We investigated possible orbits of the satellite galaxy that can form stellar shells. The formation of the stellar shells is common in almost radial mergers, which we presented in Paper I, for different satellite morphologies. In this paper, we present the influence of initial velocity, and consequently deviation from radial orbit, on stellar shells formation in the halo of the host.

We ran pure N-body simulations for 4 Gyrs, and we used a spherical satellite galaxy and an M31-like model for the host. For several initial distances, we varied the initial velocity from 0 to 150 km/s with a step of 25 km/s. For the distance of 150 kpc, stellar shells form for initial velocity 0 km/s. The shells are prominent, and multiple shells are formed with radii up to 100 kpc. When the initial velocity is increased to 25 km/s and 50 km/s, fainter shells were formed. For distances larger than 150 kpc, shells form only in almost radial mergers. Faint structures are formed in the S3-200-25 model with an initial velocity of 25 km/s. In the S3-250-0 model, with an initial distance of 250 kpc, structures are formed only in the case of a radial merger, 2.5 Gyr after the start of the simulation. For velocities larger than 50 km/s in the S3-150 models, 25 km/s in S3-200, and 0 km/s in S3-250, the satellite galaxy will experience tidal disruption, or will orbit around the host, but without stellar shell formation.

To identify shells, we generate phase v-d plots and compare them with distributions in the x-y and x-z planes. We traced the formation of shells in the first 3 Gyrs, and compared tidal structures formed after 2.5 Gyrs for all models. Deviation from a radial orbit leads to formation of faint stellar structures, and these phase plots confirm the intensity and number of formed shells. In the other direction, for the observed stellar shells, we can find an upper limit for the initial tangential velocity for a given initial distance, which still allows shell formation. In merger models, it is not necessary to have a radial orbit for shell formation, especially in the case of a very faint stellar shell with a small radius. Combination of initial parameters, like the initial distance and velocity, gives possible scenarios for stellar shell formation that deviate from the radial orbit, and they are given in Fig. 5, Fig. 6, and Fig. 12. For the initial distance of 150 kpc, shells are formed for the initial velocities up to 50 km/s, for 200 kpc, up to 25 km/s, and for 250 kpc only for 0 km/s, all in the first 2.5 Gyrs after the beginning of the simulation. These results are confirmed in Fig. 7, Fig. 8 and Fig. 13, where we presented formation of

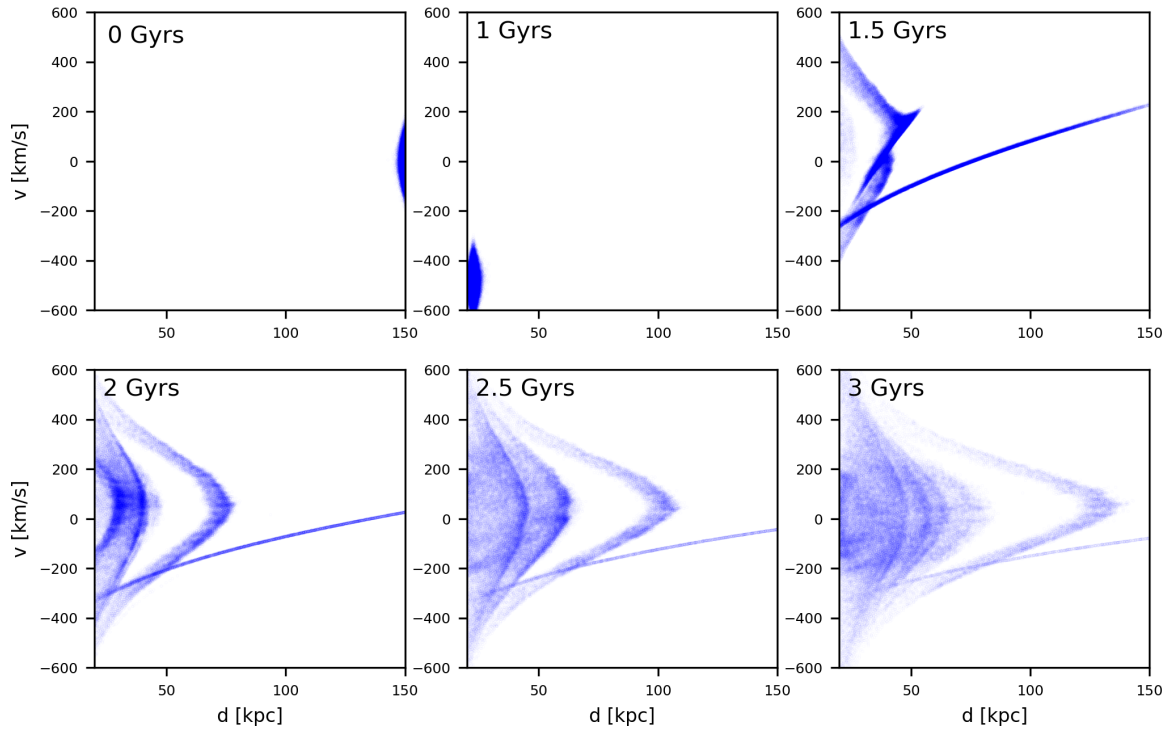

Fig. 9: The phase-space plots for the time interval between 0 and 3 Gyrs, for the S3-150-0 model. There are several formed shells and a stellar stream.

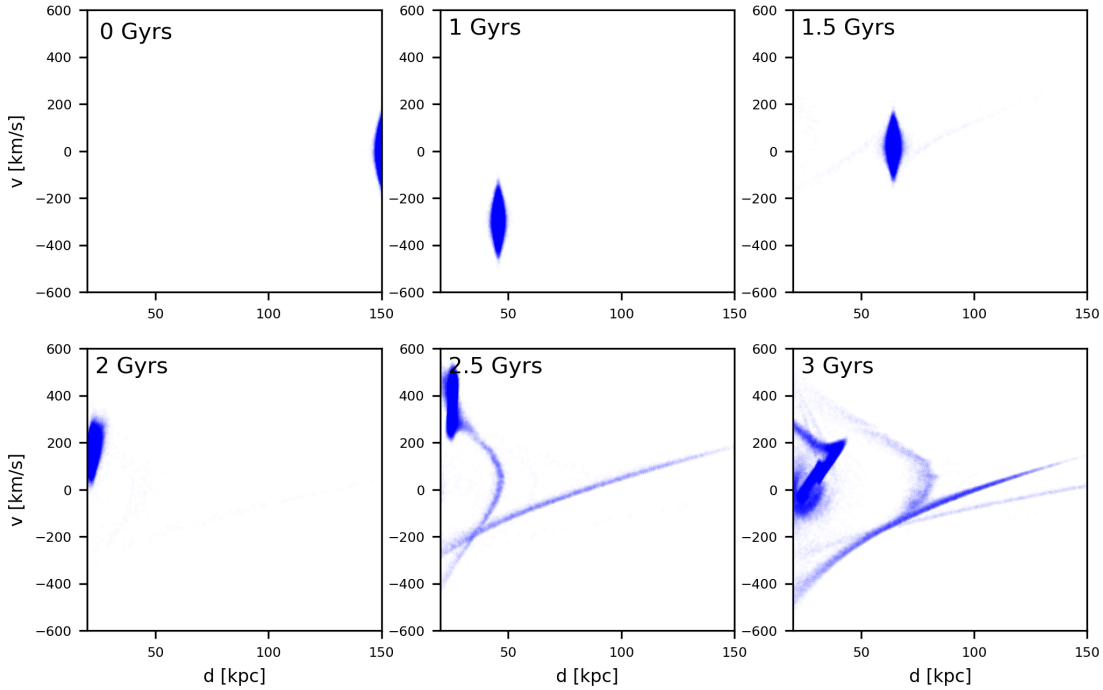

Fig. 10: The phase-space plots for the time interval between 0 and 3 Gyrs for the S3-150-50 model. With the initial velocity 50 km/s, we have less prominent shells that are formed later in the merger.

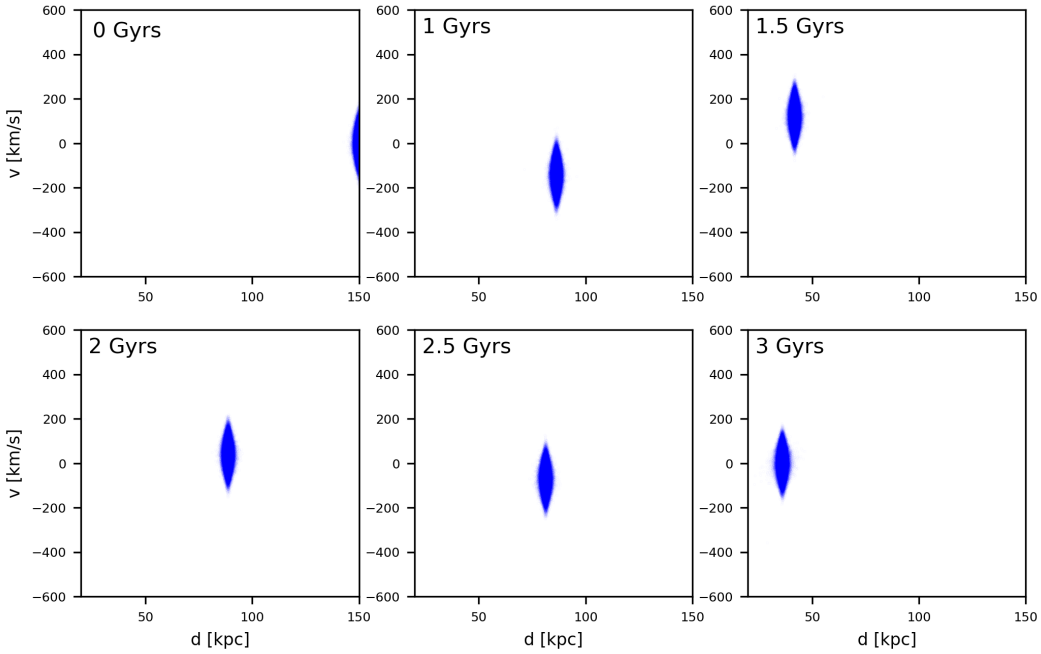

Fig. 11: Merger history for the S3-150-100 model.

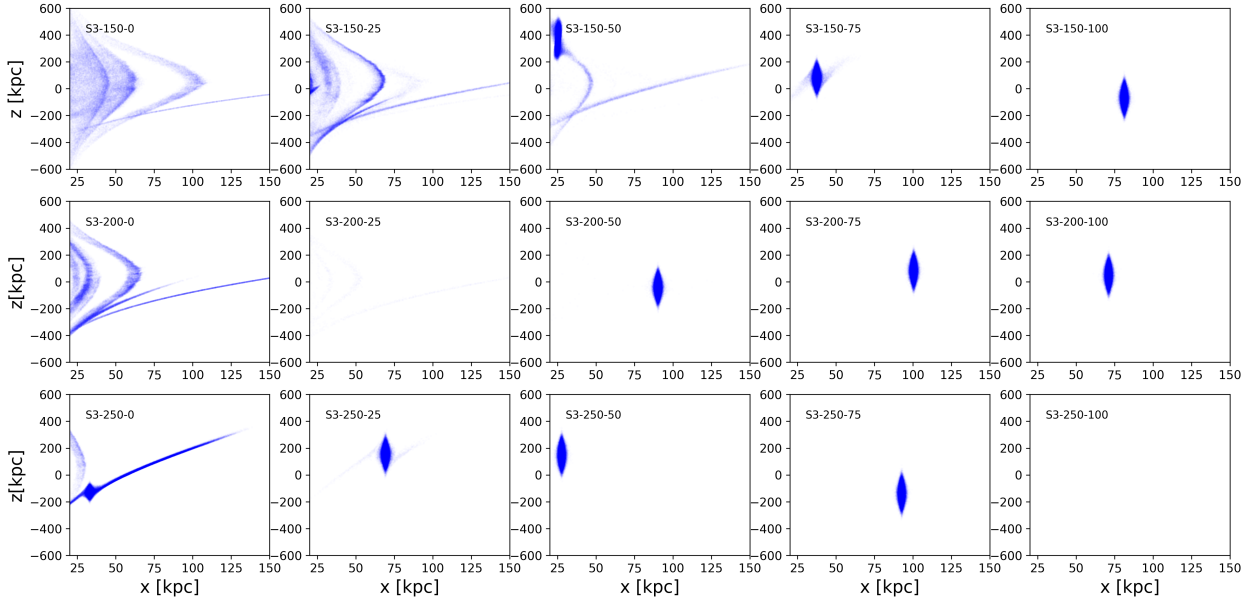

Fig. 12: The phase-space plots at 2.5 Gyrs from the beginning of the simulation. The upper row represents models with initial distance of 150 kpc, and for initial velocities from 0 to 100 km/s, with a step of 25 km/s. The middle row is for models with initial distance of 200 kpc, and the bottom row is for initial distance of 250 kpc. Symbols and panels correspond to the panels in Fig. 5 and Fig. 6.

tidal structures at time 1 Gyr after the first pericentric passage.

Observed properties and detected stellar shells, or lack of the shells, can constrain possible orbits and initial velocity of the satellite galaxy at the beginning of the accretion onto the host (Hendel and Johnston 2015). In combination with results and statistics of large cosmological simulations, where merger histories are known, the initial conditions for a halo tidal structure formation, and parameters for numerical simulations can be better constrained. This will be a part of our future work.

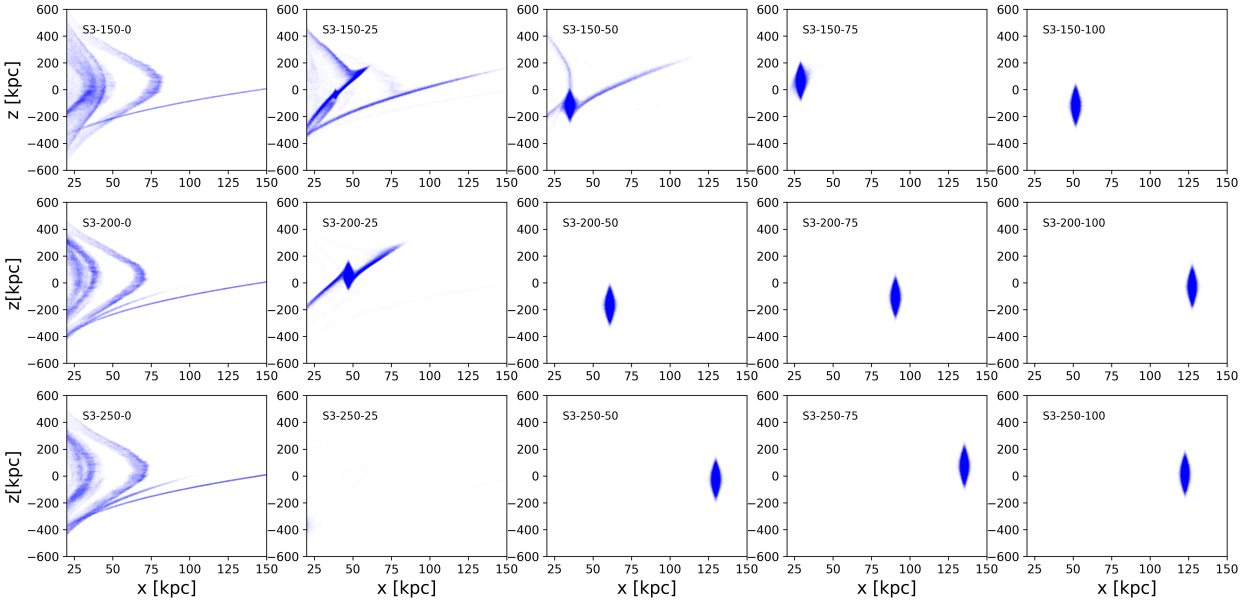

Fig. 13: The phase-space plots at 1 Gyr after the first pericentric passage. The upper row represents the models with initial distance of 150 kpc and for initial velocities from 0 to 100 km/s, with a step of 25 km/s. The middle row is for the models with initial distance of 200 kpc, and the bottom row is for initial distance of 250 kpc. Symbols and panels correspond to the panels in Fig. 7 and Fig. 8.

Acknowledgements – We thank the reviewer for a helpful discussion and comments. This work was supported by the Ministry of Science, Technological Development, and Innovation of the Republic of Serbia through contract: 451-03-33/2026-03/200104

REFERENCES

Amorisco, N. C. 2015, MNRAS, 450, 575
Arp, H. 1966, ApJS, 14, 1
Atkinson, A. M., Abraham, R. G. and Ferguson, A. M. N. 2013, ApJ, 765, 28
Behroozi, P. S., Wechsler, R. H. and Conroy, C. 2013, ApJ, 770, 57
Belokurov, V., Zucker, D. B., Evans, N. W., et al. 2006, ApJL, 642, L137
Bílek, M., Cuillandre, J.-C., Gwyn, S., et al. 2016, A&A, 588, A77
Bílek, M., Fensch, J., Ebrová, I., et al. 2022, A&A, 660, A28
Bullock, J. S. and Johnston, K. V. 2005, ApJ, 635, 931
Cole, S., Lacey, C. G., Baugh, C. M. and Frenk, C. S. 2000, MNRAS, 319, 168
Cooper, A. P., Cole, S., Frenk, C. S., et al. 2010, MNRAS, 406, 744
de Blok, W. J. G., Józsa, G. I. G., Patterson, M., et al. 2014, A&A, 566, A80
Dressler, A. 1980, ApJ, 236, 351
Ebrova, I. 2013, arXiv:1312.1643
Ebrová, I., Jílková, L., Jungwiert, B., et al. 2012, A&A, 545, A33
Ebrová, I., Bílek, M., Yıldız, M. K. and Eliášek, J. 2020, A&A, 634, A73
Escala, I., Gilbert, K. M., Wojno, J., Kirby, E. N. and Guhathakurta, P. 2021, AJ, 162, 45
Fardal, M. A., Guhathakurta, P., Babul, A. and McConnachie, A. W. 2007, MNRAS, 380, 15
Fardal, M. A., Guhathakurta, P., Gilbert, K. M., et al. 2012, MNRAS, 423, 3134
Ferguson, A. M. N., Irwin, M. J., Ibata, R. A., Lewis, G. F. and Tanvir, N. R. 2002, AJ, 124, 1452
Geehan, J. J., Fardal, M. A., Babul, A. and Guhathakurta, P. 2006, MNRAS, 366, 996
Hammer, F., Yang, Y. B., Wang, J. L., et al. 2018, MNRAS, 475, 2754
Hendel, D. and Johnston, K. V. 2015, MNRAS, 454, 2472
Hernquist, L. and Quinn, P. J. 1987, ApJ, 312, 1
Hernquist, L. and Quinn, P. J. 1988, ApJ, 331, 682
Hernquist, L. and Quinn, P. J. 1989, ApJ, 342, 1
Ibata, R. A., Gilmore, G. and Irwin, M. J. 1994, Natur, 370, 194
Johnston, K. V., Hernquist, L. and Bolte, M. 1996, ApJ, 465, 278
Johnston, K. V., Sigurdsson, S. and Hernquist, L. 1999, MNRAS, 302, 771
Karademir, G. S., Remus, R.-S., Burkert, A., et al. 2019, MNRAS, 487, 318
Klypin, A., Kravtsov, A. V., Valenzuela, O. and Prada, F. 1999, ApJ, 522, 82
Kruijssen, J. M. D., Pfeffer, J. L., Chevance, M., et al. 2020, MNRAS, 498, 2472
Martínez-Delgado, D., Gabany, R. J., Crawford, K., et al. 2010, AJ, 140, 962
Milošević, S. 2022, SerAJ, 205, 33
Milošević, S., Mićić, M. and Lewis, G. F. 2022, MNRAS,

511, 2868
Moore, B., Ghigna, S., Governato, F., et al. 1999, ApJL, 524, L19
Navarro, J. F., Frenk, C. S. and White, S. D. M. 1996, ApJ, 462, 563
Petersson, J., Renaud, F., Agertz, O., Dekel, A. and Duc, P.-A. 2023, MNRAS, 518, 3261
Pop, A.-R., Pillepich, A., Amorisco, N. C. and Hernquist, L. 2018, MNRAS, 480, 1715
Quinn, P. J. 1984, ApJ, 279, 596
Sadoun, R., Mohayaee, R. and Colin, J. 2014, MNRAS, 442, 160
Schweizer, F. and Ford, Jr., W. K. 1985, in New Aspects of Galaxy Photometry, ed. J. L. Nieto, Vol. 232, 145
Springel, V. 2005, MNRAS, 364, 1105
Tempel, E., Saar, E., Liivamägi, L. J., et al. 2011, A&A, 529, A53
Valenzuela, L. M. and Remus, R.-S. 2024, A&A, 686, A182
White, S. D. M. and Frenk, C. S. 1991, ApJ, 379, 52
White, S. D. M. and Rees, M. J. 1978, MNRAS, 183, 341
Widrow, L. M., Pym, B. and Dubinski, J. 2008, ApJ, 679, 1239

МОГУЋЕ ОРБИТЕ ГАЛАКСИЈЕ САТЕЛИТА ПРИ ФОРМИРАЊУ ЗВЕЗДАНИХ ЉУСКИ У СУДАРИМА ГАЛАКСИЈА

С. Милошевић

Катедра за астрономију, Математички факултет, Универзитет у Београду, Студентски трг 16, 11000 Београд, Србија

E–mail: *stanislav.milosevic@matf.bg.ac.rs*

УДК 524.74 : 519.876
Оригинални научни рад

У овом раду истражујемо формирање звезданих љуски, насталих у сударима спиралне галаксије са сфероидном галаксијом која је њен сателит. Звездане љуске се формирају у сударима који су скоро радијални и у овом раду је тестирано колико орбита може да одступа од радијалне, а да се љуске ипак формирају. Извршене су симулације N тела судара галаксије која има структуру као M31 галаксија и сфероидне галаксије сателита. Симулације су извршене за временски интервал од 4 милијарде година. Са почетном брзином до 50 km/s, у овим ударним сценаријима, се формирају звездане љуске за почетну удаљеност од 150 kpc; затим у сударима са почетном брзином сателита до 25 km/s за удаљеност од 200 kpc и за почетну удаљеност од 250 kpc, звездане љуске се формирају само у радијалним сударима након 2,5 милијарди година од почетка симулације. Путање дефинисане почетном брзином од 100 km/s и већом, узрокују сударе који не воде формирању љуски, или пак не долази до судара.